Flow and Heat Transfer Processes in an Inertance type Pulse Tube Refrigerator

D. Antao and B. Farouk

Department of Mechanical Engineering and Mechanics
Drexel University
Philadelphia, PA 19104

ABSTRACT

A time-dependent axisymmetric (r-z) numerical study is reported here for the investigation of the fundamental flow and heat transfer processes found in an inertance type pulse tube refrigerator (IPTR). The general design of an IPTR incorporates a pressure wave generator, a transfer line, an aftercooler, a regenerator, a pulse tube, a pair of heat exchangers for the cold and hot ends of the pulse tube, an inertance tube and a reservoir. The performance of the IPTR system is simulated using computational fluid dynamics (CFD). The IPTR is driven by a cyclically moving piston at one end of the system operating at a fixed frequency with helium as the working fluid. Both constant temperature and convective heat transfer boundary conditions are examined along the external walls of the hot heat exchangers. The simulations reveal interesting time-dependent flow patterns that develop in the pulse tube due to the fluctuations caused by the piston and the presence of the inertance tube. The secondary-flow recirculation patterns in the pulse tube reduce the heat pumping effect from the low-temperature heat exchanger to the high-temperature heat exchangers.

INTRODUCTION

Thermoacoustic refrigerators have attracted renewed attention lately as they eliminate the need for harmful refrigerants such as CFCs. The small number of moving parts required makes them simple and hence potentially very reliable. The pulse tube refrigerator is an interesting type of thermo-acoustic device and was first discovered and reported by Gifford and Longsworth in 1964.[1,2] They named the device 'pulse tube refrigerator' as the displacer (found in Stirling and GM cryocoolers) was replaced by a tube. The word *pulse* is derived from the fact that pressure pulses are used to compress and expand the gas (converted to heating and cooling respectively). This initial pulse tube refrigerator design is now called a Basic Pulse Tube refrigerator (BPTR). Initial experiments using Helium as the working gas resulted in cold temperatures of around 169 K for a single stage and 123 K for a double-stage cryocooler. In 1984, Mikulin[3] demonstrated that the phase and amplitude relation between velocity and temperature can be managed by controlling the boundary conditions at the end of the pulse tube. This was done by placing an orifice and a reservoir (compliance/surge) volume at the end of the BPTR thus allowing a finite gas flow. The presence of the orifice changes the phase angle between the velocity and temperature at the cold end and increases enthalpy flow at the hot end. Mikulin's initial experiments attained 105 K with air as the working

Cryocoolers 16, edited by S.D. Miller and R.G. Ross, Jr.

gas. This was the first Orifice Pulse Tube refrigerator (OPTR). The OPTR results in lower temperatures, increased cooling and higher efficiencies than the BPTR.

Radebaugh at NIST (Boulder, CO) worked on the OPTR as it is known today. His initial work recorded temperatures around 60 K.[4] Recent variations of the OPTR include the addition of an extra orifice creating a double-inlet pulse tube and the addition of an inertance tube. The double-inlet allows the gas to be compressed from the hot end of the tube also, thus increasing the phase angle and reducing the flow through the regenerator (which reduces enthalpy flow losses). The term, inertance, is a combination of the words inertia and inductance (analogous to the inductance in an electrical circuit).[5] The idea of using an inertance tube is to use the inertia of the gas to provide an added phase shift in a long tube. The inertance tube can be used instead of an orifice or in addition to one. Marquardt and Radebaugh reported the highest efficiency for the pulse tube refrigerator when using a combination of the orifice and the inertance tube.[6]

1-D computational models have been widely used for modeling thermoacoustic devices. Swift[7,8,9] developed a 1-D code for the entire PTR system (and other thermoacoustic engines and refrigerators) based on Rott's[10] linear acoustic equations. While the 1-D codes provide relatively good estimations of various operating parameters of the PTR (dimensions, operating frequencies, etc.), they use idealistic assumptions and do not reflect the multidimensional nature of the flow and transport inside the PTR systems.

Lee[5] developed a set of 2-D differential equations for use in describing the steady secondary flows generated by the periodic compression and expansion of an ideal gas in pulse tubes. The equations were used to obtain an insight into the physics of the pulse tube in a BPTR and an OPTR for what is known as the thermally strong case. More recently, Flake and Razani[11] carried out an axisymmetric analysis of a BPTR and an OPTR and showed cycle-averaged flow patterns in the pulse tube. Cha[12] studied two IPTR systems based on the geometry of the pulse tube (for two values of L/D ratios). They showed the formation of vortical structures in the pulse tube for the small L/D case which had a negative effect on the cooling due to the mixing of flow in the pulse tube. Ashwin[13] studied the effect of using a thermal non-equilibrium model in the porous media (heat exchangers and regenerator) and the effect of considering a finite wall thickness for the various components of the IPTR. The effect of a finite wall thickness was found to increase the steady state temperature at the cold end of the pulse tube due to the heat conduction along the walls of the pulse tube from the hot end to the cold end.

In this paper, we report time-dependent axisymmetric (r-z) CFD simulations where the transient as well as the steady-periodic (cycle-averaged) operation of an IPTR is studied. One of the objectives is to study the effect of applying realistic boundary conditions to the system and comparing it to the ideal boundary conditions studied earlier. A second objective is to study the cycle-averaged secondary flows that exist in the pulse tube and how they affect the performance of the system.

SCHEMATIC OF PROBLEM GEOMETRY

Figure 1 depicts the simulation domain for the computations performed on the IPTR. The axisymmetric configuration for the IPTR consists of a compression chamber (which includes the moving piston), the transfer tube, aftercooler, regenerator, pulse tube with two heat exchangers at its ends, an inertance tube and the compliance volume. The dimensions of the system were adopted based on past work by Cha[12] and Banjare.[14]

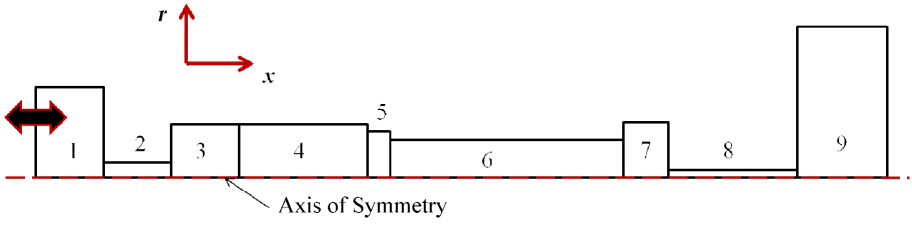

Figure 1. Schematic of the problem geometry in the simulations.

Table 1 summarizes the dimensions of the problem geometry and the static boundary conditions. The boundary conditions at the components' surfaces will be explained in detail in a following section.

MATHEMATICAL MODEL

The flow and heat transfer simulation model incorporates the fluid dynamic equations of conservation of mass (continuity equation), momentum and energy in the fluid domain. The various heat exchangers and the regenerator are modeled as porous media with the relevant solid properties of the regenerator and the heat exchanger materials.

The fluid in the system is helium. Helium was assumed to be an ideal gas and its viscosity and thermal conductivity were assumed to be temperature dependent. The specific heat was kept constant since it does not vary considerably in the temperature range studied (i.e. 350 K – 100 K). The temperature dependent properties were obtained from the NIST database.[15]

In the heat exchangers (considered as porous media) the solid phase considered was copper. The density and specific heat of copper were assumed to be 8950 kg/m^3 and 380 J/kg-K respectively and the thermal conductivity was assumed to have two values based on the temperature range of operation (i.e. 401 W/m-K from 350 – 200 K and 470 W/m-K from 200 – 100 K). Similarly for the regenerator (considered as porous media), stainless steel was considered as the solid phase and the density and specific heat were assumed to be 7810 kg/m^3 and 460 J/kg-K respectively and the thermal conductivity was assumed to have two values based on the temperature range of operation (i.e. 20 W/m-K from 350 – 200 K and 10 W/m-K from 200 – 100 K).

Governing Equations

In the fluid regions (helium), the conservation equations are as follows:

$$\frac{\partial \rho}{\partial t} + \nabla \cdot (\rho \vec{u}) = 0 \tag{1}$$

$$\frac{\partial (\rho \vec{u})}{\partial t} + \nabla \cdot (\rho \vec{u}\vec{u}) = -\nabla p + \nabla \cdot \tau_{ij} \tag{2}$$

$$\frac{\partial (\rho h_0)}{\partial t} + \nabla \cdot (\rho \vec{u} h_0) = \frac{\partial p}{\partial t} + \nabla \cdot (k \nabla T) + \nabla (\vec{u} \tau_{ij}) \tag{3}$$

where,

$$h_0 = i + \frac{p}{\rho} + \frac{1}{2}\left(\vec{u}\right)^2 \tag{4}$$

Local thermodynamic equilibrium is assumed to exist between the fluid and porous media. The mass, momentum and energy equations solved in the porous media are given as follows:

$$\frac{\partial (\varepsilon \rho)}{\partial t} + \nabla \cdot (\varepsilon \rho \vec{u}) = 0 \tag{5}$$

Table 1. Dimensions and boundary conditions of the simulated system

No.	Component	Radius (m)	Length (m)	Boundary Condition
1	Compression Chamber	0.00954	0.0075	Adiabatic
2	Transfer Tube	0.00155	0.101	hc = 200 W/m-K
3	Aftercooler	0.004	0.02	Variable
4	Regenerator	0.004	0.058	Adiabatic
5	Cold HX	0.003	0.0057	Adiabatic
6	Pulse Tube	0.0025	0.06	Adiabatic
7	Hot HX	0.004	0.01	Variable
8	Inertance Tube	0.0005	0.13	Adiabatic
9	Compliance Volume	0.013	0.13	Adiabatic

$$\frac{\partial\left(\varepsilon\rho\vec{u}\right)}{\partial t}+\nabla\cdot\left(\varepsilon\rho\vec{u}\vec{u}\right)=-\varepsilon\nabla p+\nabla\cdot\left(\varepsilon\tau_{ij}\right)-\frac{\varepsilon^2\mu}{\kappa}\vec{u}-\frac{\varepsilon^3 C_F\rho}{\sqrt{\kappa}}\left|\vec{u}\right|\vec{u} \tag{6}$$

$$\frac{\partial\left(\varepsilon\rho h_0\right)}{\partial t}+\nabla\cdot\left(\varepsilon\rho\vec{u}h_0\right)=\nabla\cdot\left(k_{eff}\nabla T\right)+\nabla\left(\varepsilon\vec{u}\tau_{ij}\right)+\varepsilon\frac{\partial p}{\partial t} \tag{7}$$

and

$$k_{eff}=-2k_s+\frac{1}{\dfrac{\varepsilon}{2k_s+k_f}+\dfrac{1-\varepsilon}{3k_s}} \tag{8}$$

where, ε is the porosity of the porous media and has a value of 0.69. The permeability (κ) is assumed to be 1.06 ×10"4 m^2 and the quadratic drag factor (C_F) has a value of 0.55. The values of porosity and permeability were assumed based on the work of Cha[12] and Harvey.[16]

Boundary and Initial Conditions

Boundary Conditions: Table 1 specifies the boundary conditions used at the various components' surfaces. The two cases studied were for different temperature boundary conditions at the aftercooler and the hot heat exchanger.

Case 1: Aftercooler and Hot HX have constant temperatures of 293 K and

Case 2: Aftercooler and Hot HX have convective heat transfer coefficients (h_c) at their surfaces. The value of h_c used was 1000 W/m^2-K, which is equivalent to having water cooled heat exchanger with a flow velocity of around 0.2 – 0.3 m/s.

The piston is modeled as a reciprocating wall having an oscillatory velocity. The velocity of the piston is defined by the function, $u = A_0\omega Cos(\omega t)$, where A_0 is the maximum displacement of the piston (4.511 mm) and ω is the angular frequency ($\omega = 2\pi f$) and f is the frequency of operation. For the simulations f is assumed to be 34 Hz.

Initial Conditions: At the start, the temperature in the system was assumed to be 300 K. The operating pressure in the system was set to 3.1 MPa.

Numerical Scheme

The above governing equations and the boundary conditions were solved using CFD-ACE+.[17] The numerical scheme for solving the governing equations is based on the finite volume approach. The continuity, momentum and energy equations are solved for the fluid as well as the porous media using a 2nd order upwind scheme. A 1st order Euler scheme is used for the time derivatives in the continuity, momentum and energy equations with a time-step size equal to 3.65 ×10^{-4} s. The time marching calculations are continued until the cycle averaged variation in the cold end temperature is within 5 % of the value from the previous time-step. At this time, the time averaged velocity in the pulse tube has attained a steady value. The solutions are then considered to be quasi-steady.

An overall convergence criterion is set for all the variables at 0.001 and the convergence criterion for the energy equation is set at 0.0001.

GRID STRUCTURE

Due to the symmetry of the problem geometry, 2-D cylindrical axisymetric simulations were performed to save computation time. A hybrid grid structure is used in the simulations with higher density mesh used at the various junctions of the different components. Figure 2 shows some the grid structures used in the simulations. Structured grid (non-uniform orthogonal mesh) was used in all components except the cold heat exchanger at the beginning of the pulse tube. In this heat exchanger, the grid structure used was an unstructured triangular mesh. This was done to capture the true flow and transport effects at the junction of the Cold HX and the Pulse tube as well as the junction of the Regenerator and Cold HX. A total of 4710 grid points were used in the system.

Figure 2. Grid Structure in the Cold HX, the Pulse tube and the Hot HX.

RESULTS AND DISCUSSION

Transient Processes in the System

The processes in an inertance type pulse tube refrigerator are mainly transient in nature and the cool-down process is shown in Figure 3. Figure 3 shows the temperature at the exit of the cold heat exchanger and in the hot heat exchanger as a function of time for the two cases studied. The solid lines in the figure represent the Cold HX temperature and the dashed lines represent the temperatures in the Hot HX.

It can be clearly seen that the temperature in case 2 is higher than that in case 1. The higher temperature at the cold end is due to the fact that not enough heat is being removed from the hot heat exchanger at the end of the pulse tube.

Figure 4 shows the pressure and temperature profiles at the entrance of the pulse tube at the start of the simulation (the first four cycles are shown) for case 1. The pressure exhibits a fairly sinusoidal pattern; however the temperature profile is distorted. This plot also shows a steep decrease/drop in the temperature at the beginning of the process. As the simulation progresses, the temperature drops from cycle to cycle decrease exponentially.

Spatial Temperature Profiles

In Figure 5, we show the axial distribution of the temperature in the system along the line of symmetry (i.e. $r = 0$ in the simulations) for case 1 studied. The four plots in the figure indicate the temperature profile at four points in the cycle (1764th) i.e. 0 (or 2π), $\pi/2$, π and $3\pi/2$. The temperature is shown for the transfer tube up till the hot end of the pulse tube. Beyond the hot heat exchanger, the temperature barely oscillates and is about 295 K. The temperature profile along the regenerator and the pulse tube do not have linear profiles. A possible reason for this is that the system has not fully attained as steady-cyclic mode.

Steady-State Multidimensional Effects

In Figure 6 and 7, the time-averaged temperature and velocity profiles in the regenerator and the pulse tube respectively at the 1764th cycle (case 1) are shown. By this time, the system is assumed to have reached a relatively steady state ($\Delta T \sim 0.1$ K/cycle).

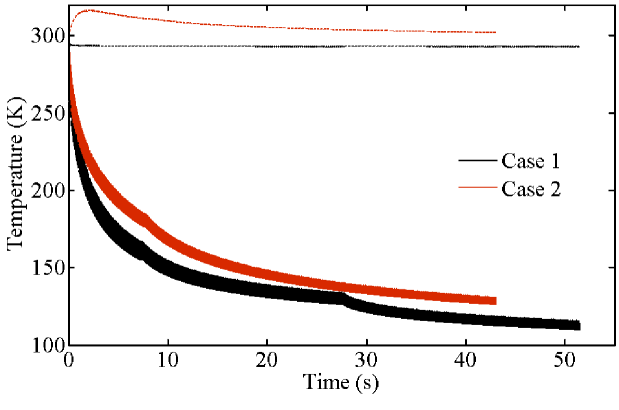

Figure 3. Transient evolution of the temperature at the entrance to the pulse tube. The dotted lines indicate the temperature at the exit of the pulse tube (hot heat exchanger). *Case 1*: Aftercooler and Hot HX have constant temperatures of 293 K and *Case 2*: Aftercooler and Hot HX have convective heat transfer coefficients ($h_c = 1000$ W/m^2-K) at their surfaces.

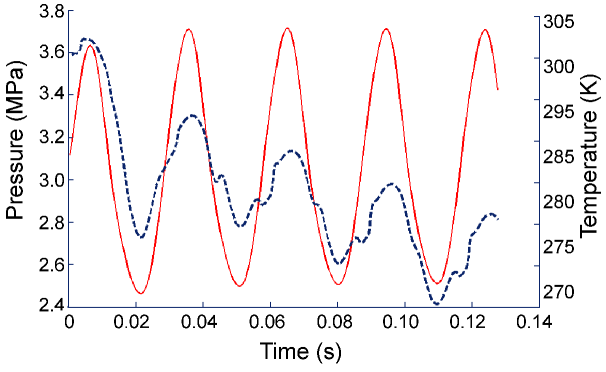

Figure 4. Temperature and Pressure profiles at the early stage of the simulation (Cycles 1 – 4) for Case 1.

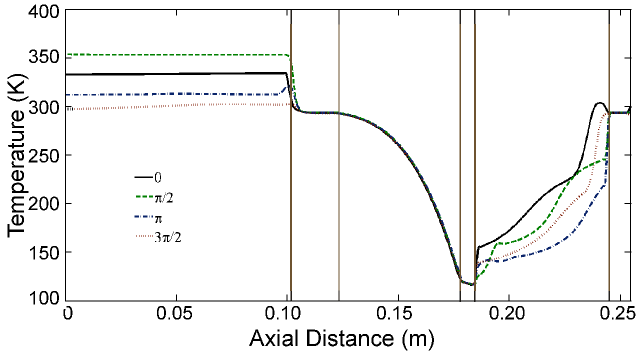

Figure 5. Axial distribution of the temperature (along the axis of symmetry) at four different times in cycle 1764 for case 1. The vertical lines demarcate the different components (from left to right: transfer tube, aftercooler, regenerator, cold heat exchanger, pulse tube and hot heat exchanger).

The flow and temperature fields in the pulse tube are explored next. Figure 7 show the cycle-averaged temperature field and streamlines in the pulse tube (see Figure 1). While the flow field in the pulse tube is oscillatory the cycle-averaged flow field shows remarkable organization. The cycle-averaged flow field is characterized by two sets of counter-rotating vortex pairs. One set of rolls on the cold end side of the pulse tube is larger and a smaller set of rolls is observed on the hot end side. The maximum streaming velocity in the axial direction is around 1.84 m/s and the minimum is around -2.65 m/s (the negative sign indicates flow in the negative x-direction), however the bulk of the streaming velocity is around 0.1 and -0.1 m/s. The maximum and minimum velocities in the radial direction are 0.72 m/s and -0.13 m/s. The temporal flow field in the pulse tube shows a stream of flow oscillating along the axis of the pulse tube. This stream brings hot fluid from the hot heat exchanger to a colder section of the pulse tube in a cyclic manner through the gas plug in the center of the pulse tube.

In order to explain the significance of the streaming profile, we reexamine the processes in the pulse tube as proposed by Radebaugh.[18] It is well known that the main function of the pulse tube is to insulate the processes at its two ends. The pulse tube must be large enough that the gas flowing from the warm end traverses only half way through the pulse tube before flow is reversed. Similarly, the flow entering from the cold end should never reach the warm end. Gas in the middle portion of the pulse tube ideally never leaves the pulse tube and forms a temperature gradient that insulates the two ends. Radebaugh proposed that the entire cycle in an OPTR or an IPTR can be simplified to the following four steps:

1. The piston in the compressor compresses the gas in the pulse tube.

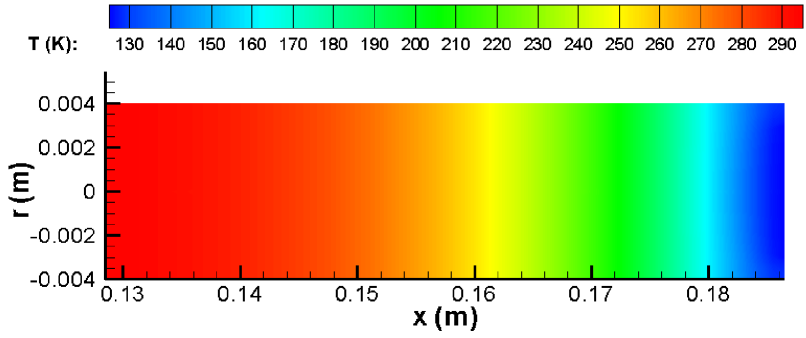

Figure 6. Cycle averaged temperature profile in the regenerator section (Case 1).

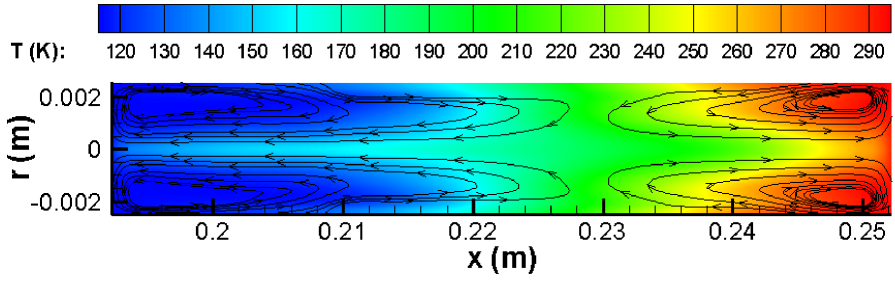

Figure 7. Cycle-averaged temperature and streamlines in the pulse tube section (Case1).

2. Due to compression, the gas is heated and is at a higher pressure than the average in the reservoir. This high pressure gas then flows through the orifice into the reservoir and exchanges heat with the ambient through the heat exchanger at the warm end of the pulse tube. The flow stops when the pressure in the pulse tube is reduced to the average pressure.
3. The piston in the compressor expands the gas adiabatically in the pulse tube.
4. The cold low-pressure gas (due to expansion) in the pulse tube is forced toward the cold end by the gas flow from the reservoir into the pulse tube through the orifice. As the cold gas flows through the heat exchanger at the cold end of the pulse tube it picks up heat from the object being cooled. The flow stops when the pressure in the pulse tube increases to the average pressure.

Based on our simulations, the animations of the flow in the pulse tube exhibit a similar set of four processes as proposed by Radebaugh. A buffer zone is also visible (seen in green between 0.228 m and 0.23 m in Figure 7) and is seen to oscillate within the pulse tube. However, the animations also show a leakage flow along the axis of symmetry in the simulations. This leakage flow moves from the thermal buffer region (seen in green in Figure 7) in the pulse tube to the two ends of the pulse tube. The presence of two sets of symmetric rolls near the cold end and near the hot end causes a recirculation of the flow in the pulse tube. Each recirculation flow pulls the fluid from the buffer region to the cold end and hot end and recirculates the flow from the ends of the tube to the buffer region. This recirculation prevents the cold end from reaching the coldest temperature possible. Thus studying the problem of cycle averaged streaming in the pulse tube can lead to the design of more efficient pulse tube refrigerators.

SUMMARY

The flow and temperature fields in an IPTR system were simulated for two sets of boundary conditions. It was shown that effective cooling is required in the heat exchangers to ensure optimum operation of the IPTR (to attain the lowest temperature possible). Cycle-averaged tempera-

ture and velocity profiles were obtained for the pulse tube and regenerator sections of the IPTR system. The cycle averaged velocity profiles in the pulse tube indicate the presence of steady streaming recirculation patterns. These steady streaming velocities produce a recirculation flow in the pulse tube which leads to a deterioration in the IPTR system performance.

ACKNOWLEDGMENT

This project is supported by the National Science Foundation under the grant CBET-0853959.

REFERENCES

1 Gifford, W. E., and Longsworth, R.C., “Pulse-tube refrigeration,” Trans. Of the ASME, Journal of *Engineering for Industry*, paper No. 63-WA-290, August 1964., pp. 264-268

2. Gifford, W. E., and Longsworth, R.C., "Pulse tube refrigeration progress," *Adv. in Cryogenic Engineering,* Vol. 10, Plenum Publishing Corp., New York (1965), pp. 69-79

3. Mikulin, E.I., Tarasov, A.A., and Shkrebyonock, M.P., "Low-Temperature Expansion Pulse Tubes," *Adv. in Cryogenic Engineering,* Vol. 29, Plenum Publishing Corp., New York (1984), pp. 629-637.

4. Radebaugh, R., Zimmerman ,J., Smith, D.R., and Louie, B., "A Comparison of three types of Pulse Tube Refrigerators: New methods for reaching 60 K," *Adv. in Cryogenic Engineering,* Vol. 31, Plenum Publishing Corp., New York (1986), pp. 779-789.

5. Lee, J.M., "Steady Secondary Flows Generated by Periodic Compression and Expansion of an Ideal Gas in a Pulse Tube," Ph.D. dissertation, University of Colorado, Boulder, 1997.

6. Marquardt, E.D., and Radebaugh, R., “Pulse Tube Oxygen Liquefier,”*Adv. in Cryogenic Engineering,* Vol. 45, Plenum Publishing Corp., New York (2000), pp. 457-464.

7. Swift, G.W., “Thermoacoustic Engines,” *J. Acoust. Soc. America*, vol. 84, no. 4 (1988), pp. 1145 - 1180

8. Swift, G.W., *Thermoacoustics: A Unifying Perspective for Some Engines and Refrigerators*, Acoustical Society of America, Melville, NY (2002)

9. "Design Environment for Low-amplitude Thermoacoustic Energy Conversion, DeltaEC, **v.** 6.2, User's Guide," LA-CC-01-13, Los Alamos National Labs, December 8, 2008.

10. Rott, N., *Thermoacoustics*, Academic Press, New York (1980), pp. 135

11. Flake, B., and Razani, A., "Modeling pulse tube cryocoolers with CFD,"*Adv. in Cryogenic Engineering*, Vol. 49B, Amer. Institute of Physics, Melville, NY (2004), pp. 1493-1499.

12. Cha, J.S., Ghiaasiaan, S.M., Desai, P.V., Harvey, J.P. and Kirkconnell, C.S., “Multi-dimensional flow effects in pulse tube refrigerators,” *Cryogenics*, Vol. 46, Issue: 9, September 2006, pp. 658-665.

13. Ashwin, T.R., Narasimham, G., Jacob, S., “CFD analysis of high frequency miniature pulse tube refrigerators for space applications with thermal non-equilibrium model,” *Applied Thermal Engineering*, Vol. 30, Issues 2-3, February 2010, pp. 152-166.

14. Banjare, Y.P., Sahoo, R.K. and Sarangi, S.K., ″CFD Simulation of Orifice Pulse Tube Refrigerator," Proceedings of the International Conference on “Recent trends in Mechanical Engineering” (ICRTME-2007), October 4-6, 2007, Ujjain Engineering College Ujjain (M.P.), India

15. National Institute of Standards and Technology, NIST Standard Reference Database 12, **v.** 5.0

16. Harvey, J.P., "Parametric study of Cryocooler Regenerator Performance," M.S. Thesis, Georgia Institute of Technology, Atlanta, GA, 1999

17. ESI-Group, CFD-ACE+, **v.** 2009

18. Radebaugh, R., "Pulse tube cryocoolers for cooling infrared sensors," *Proceedings of SPIE*, *Infrared Technology and Applications XXVI*, Vol. 4130 (2000), pp. 363-379.